JOURNAL OF RESEARCH of the National Bureau of Standards—D. Radio Propagation
Vol. 65D, No. 5, September–October 1961

On the Analysis of LF Ionospheric Radio Propagation Phenomena*

J. Ralph Johler

Contribution From Central Radio Propagation Laboratory, National Bureau of Standards, Boulder, Colo.

(Received April 27, 1961)

Recent theoretical work which employs the classical magneto-ionic theory for a special model of the ionosphere applicable to transmission via the ionosphere at or close to grazing incidence is employed to analyze LF propagation data. The results of the analysis illustrate a practical model of the ionosphere by a detailed study of transmission via the first time-mode in particular.

1. Introduction

Recent contributions and extensions to the classical geometric-optical theory of propagation [Wait and Conda, 1958; Wait, 1960a; Johler and Walters, 1960, 1961] of LF waves about the earth provide a valuable analysis tool for the interpretation of various experimental data. This paper summarizes the mathematical formulas required to predict the field with particular emphasis on a type analysis most suitable for large scale electronic computers. Attention is focused on certain available experimental data and the results of the analysis are detailed with emphasis on technique. However, the physical phenomena which can be deduced as a result of the analysis of these data are given considerable attention to emphasize the value of the technique.

2. Mathematical Theory

A geometric-optical theory [Bremmer, 1949] can be employed with the aid of a sharply bounded model ionosphere [Johler and Walters, 1960, 1961] emplaced at various altitudes h above a spherical earth to describe the *cw* field, $E(\omega,d)$, radiated from a dipole source current moment, I_0l. It is common engineering practice at LF to relate the amplitude of the field, $|E(\omega,d)|$ to the well known concept of radiated power [Ballentine, 1924], neglecting earth losses,

$$P_r=1.6(10^{-13})\omega^2(I_0l)^2/Z_0, \tag{1}$$

where $Z_0\sim120\pi$, a constant. Such a field, $E(\omega,d)$, implies a similar Hertzian dipole receiver (vertical polarization). The total field, $E(\omega,d)$, is the sum of $j+1$ reflected ionospheric waves, $j=0, 1, 2, 3\ldots$,

$$E(\omega,d)=\sum_{j=0}^{p}E_j(\omega,d), \tag{2}$$

in which the zero order ($j=0$) reflection, $E_0(\omega,d)$ is the groundwave. Each skywave reflection, $j=1, 2, 3\ldots$, using the positive time function, exp $(i\omega t)$, can be written,

$$E_j(\omega,d)=i\omega dD_j^{-1}C \exp\ (i\omega t_j')G_j^iG_j^r\ \alpha_jF_jC_j, \tag{3}$$

where [Johler, Kellar, and Walters, 1956],

$$E_0(\omega,d)=[E_0(\omega,d)] \exp\ [-i(\omega b+\phi_c)], \tag{4}$$

and where,

$$C=I_0lb^2/4\pi\kappa d^3=(10^{-7})/d,(I_0l=1). \tag{5}$$

The local time [1] for the groundwave, t_0' is,

$$t_0'=t-b, \tag{6}$$

$$b=\eta_1d/c, \tag{7}$$

*This is a revised version of a paper presented at the Avionics Panel Meeting of the Advisory Goup for Aeronautical Research and Development (AGARD) NATO, Istanbul, Turkey, October 1960.

[1] The notion of local time was apparently introduced by Lorentz [1906, p. 57].

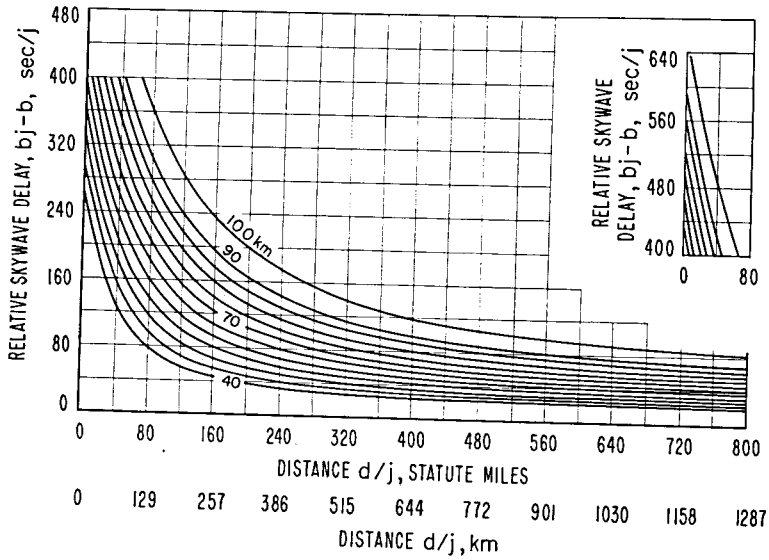

FIGURE 1. *Relative sky wave delay for various altitude,* h, *of the lower boundary of the model ionosphere.*

where c is the speed of light, $c \sim 3(10^8)$ m/sec, and η_1 is the index of refraction of air, $\eta_1 \sim 1$. Similarly, the local skywave time, or skywave delay, $t'_j (j=1, 2, 3 \ldots)$ is,

$$t'_j = t - b_j, \tag{8}$$

$$b_j = \eta_1 D_j / c, \ (j=1, 2, 3 \ldots). \tag{9}$$

The quantity, $b_j - b$, is frequently called the relative skywave delay, figure 1 (relative to the groundwave). The physical length of the ray, D_j, can be evaluated geometrically for a reflection at an altitude, h, above the surface of the earth of radius, a,

$$D_j = 2j \ [(a+h) \cos \phi_{i,j} - a \cos \tau_j], \tag{10}$$

where, figures 2, 3, ϕ_i is the angle of incidence of the "ray" on the ionosphere and τ_j is the

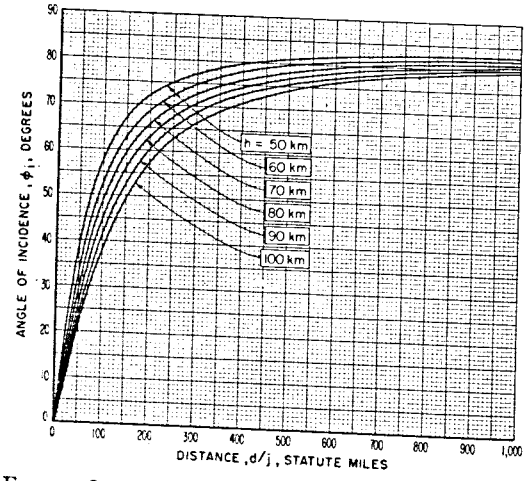

FIGURE 2. *Geometric-optical relation between the angle of incidence, ϕ_i, distance from the source, d/j (j=order of sky wave hop or time-mode, j=1, 2, 3 . . .) and altitude of the boundary of the model ionosphere,* h.

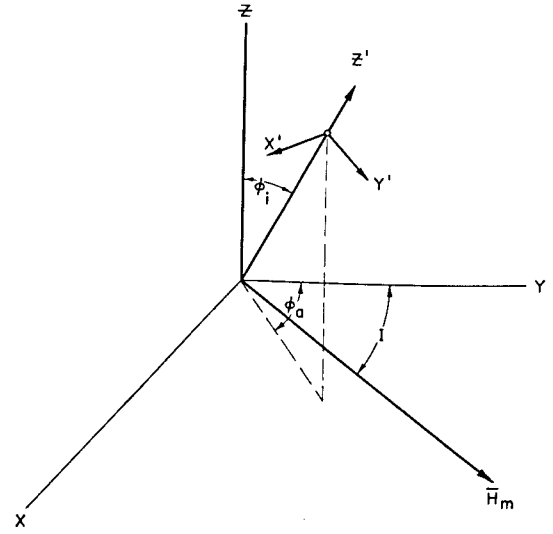

FIGURE 3. *Coordinate systems at the ionosphere boundary.*

corresponding angle of incidence on the earth and the subscript "j" reminds the reader that the equation refers to the particular ionospheric reflection under consideration. The angles ϕ_i and τ_j are evaluated quite simply from the geometry,

$$\sin \phi_{i,j}=\Delta_j^{-1}\, a \sin \frac{\theta}{2j}, \tag{11}$$

$$\cos \phi_{i,j}=\Delta_j^{-1}[a(1-\cos \theta/2j)+h], \tag{12}$$

$$\sin \tau_j=\Delta_j^{-1}(a+h) \sin \theta/2j, \tag{13}$$

$$\cos \tau_j=\Delta_j^{-1}[a(\cos \theta/2j-1)+h \cos \theta/2j), \tag{14}$$

$$\Delta_j=[2a(a+h)(1-\cos \theta/2j)+h^2]^{\frac{1}{2}}, \tag{15}$$

where θ is the angle at the center of the earth subtended by the distance, d, along the surface of a spherical earth, or, simply,

$$d=a\theta.$$

The factors, G_j^t and G_j^r refer to the transmitter and receiver complex antenna patterns respectively, and again the subscript, "j", is employed to designate the particular time-mode under consideration. The vertically polarized Hertzian dipoles considered in this paper reduce to, $G_j^t=G_j^r=\sin \tau_j$. Of course, other antenna complex pattern factors can be introduced.

Since plane reflection coefficients are employed in this analysis, the convergence-divergence coefficient, α_j, is necessary to convert the plane reflection coefficients to spherical reflection coefficients or from the viewpoint of "ray theory" it is necessary to take account of ray focusing by the ionosphere and a corresponding defocusing of rays by the earth. The "classical" convergence-divergence is modified by a "convergence correction" [Wait, 1959], A_j, in this paper, since the values of the first time-mode studied are at distances close to the "caustic" of rays or geometric-optical horizon, and hence the complete expression, α_j,

$$\alpha_j=(1+h/a)[(2j \sin \theta/2j)/\sin \theta]^{\frac{1}{2}}\times\{[a(1-\cos \theta/2j)+h]/[(a+h) \cos \theta/2j-a]\}^{\frac{1}{2}}A_j, \tag{16}$$

in which A_j can be evaluated from the cylindrical Hankel function of order, $n=\frac{1}{3}$, of the second kind,

$$A_j\sim\left[\frac{\pi}{2}k_1a \cos^3 \tau_j/3 \sin^2 \tau_j\right]^{\frac{1}{2}} H_{\frac{1}{3}}^{(2)}\left[k_1a \cos^3 \tau_j/3 \sin^2 \tau_j\right] \times\exp\left\{-i\left[5\pi/12-k_1a \cos^3 \tau_j/3 \sin^2 \tau_j\right]\right\}. \tag{17}$$

The factor,$|A_j$, approaches unity ($A_j\sim1$) at shorter distances, ($\tau_j\ll\pi/2$). Near the geometric-optical-horizon, $\tau_j\sim\pi/2$, and beyond, the correction becomes quite appreciable. The Hankel functions, $H_n^{(2)}(z)$ can be readily evaluated on an electronic computer by a consideration of the integral form,

$$H_n^{(2)}(z)=\frac{1}{\pi}\int_0^{\pi}\exp(-iz \sin \rho+in\rho)d\rho-\frac{1}{\pi i}\int_0^{\infty}\exp(-z \sinh \rho)\{\exp n\rho+\exp(-n\rho+in\pi)\}d\rho, \tag{18}$$

where the order, $n=\frac{1}{3}$, and the argument, $z=k_1a \cos^3 \tau_j/3 \sin^2 \tau_j$, in which the wave number, $k_1=\omega\eta_1/c\sim\omega/c$, for the case under consideration are real numbers. Nevertheless, it is interesting to note that the method is also applicable to complex argument, z, and complex order, n, provided the multiple branches of the Hankel function are carefully considered. The following substitution is made,

$$\beta=\exp(-\rho),$$

and a resultant expression for the Hankel function.

$$H_n^{(2)}(z)=\frac{1}{\pi}\int_0^{\pi}\exp(-iz\sin\rho+in\rho)\,d\rho-\frac{1}{\pi i}\int_0^{1}\left[\beta^{-n-1}+\beta^{n-1}\exp(in\pi)\right]\exp\left[-\frac{z}{2}\left(\frac{1}{\beta}-\beta\right)\right]d\beta, \tag{19}$$

or,

$$H_n^{(2)}(z)=\int_0^{\pi}f(z,\rho,n)d\rho-\int_0^{1}f(z,\beta,n)d\beta, \tag{20}$$

is found to comprise integrals with finite limits. These integrals can then be evaluated in terms of Gaussian quadrature,[2]

$$H_n^{(2)}(z)=\sum_{m=1}^{M}W_m^{\rho}[\mathrm{Re}f(z,\rho_m,n)+i\,\mathrm{Im}\,f(z,\rho_m,n)]-\sum_{m=1}^{M}W_m^{\beta}[\mathrm{Re}f(z,\beta_m,n)+i\,\mathrm{Im}f(z,\beta_m,n)]+\epsilon(M) \tag{21}$$

$m=1, 2, 3 \ldots M$, where, $\epsilon(M)$ can be made arbitrarily small by increasing M,

where,

$$W_m^{\rho}=\pi H_m/2,$$
$$W_m^{\beta}=H_m/2,$$
$$\rho_m=\pi x_m/2+\pi/2,$$
$$\beta_m=x_m/2+1/2,$$

and the constants, x_m, of the theory of Gaussian quadrature can be evaluated as the roots of the Legendre polynomials defined by,

$$\frac{d^M}{dx}(x^2-1)^M-2^M M!P_M(x)=0, \tag{22}$$

or,

$$P_0(x)=1,$$
$$P_1(x)=x,$$
$$P_2(x)=\frac{3}{2}x^2-\frac{1}{2},$$
$$P_3(x)=\frac{5}{2}x^3-\frac{3}{2}x,$$
$$P_4(x)=\frac{35}{8}x^4-\frac{15}{4}x^2+\frac{3}{8},$$
$$\ldots, \tag{23}$$

where polynomials of higher degree are determined by the use of the recursion formula,

$$(M+1)P_{M+1}(x)+MP_{M-1}(x)-(2M+1)xP_M(x)=0. \tag{24}$$

The weight coefficients, H_m, are evaluated from the roots, x_m,

$$H_m=2/(1-x_m^2)\,[P'_M(x_m)]^2. \tag{25}$$

The factor, F_j, accounts for the presence of the earth at the transmitter (source) and receiver. If it can be assumed that the "ray" reflected by the earth is not too close or beyond the geometric-optical horizon, the Fresnel approximation of the ground reflection coefficient suffices to determine F_j, or,

$$F_j\sim[1+R_e^i(\tau_j)][1+R_e^r(\tau_j)], \tag{26}$$

[2]This type analysis has been used extensively by the author in previous papers to evaluate Fourier integrals [Johler and Walters, 1959].

where the superscripts, t and r, refer to the transmitter and receiver respectively and the subscript, e, refers to vertical polarization, and,

$$R_e(\tau_j)=\{k_2^2\cos\tau_j/k_1^2-[k_2^2/k_1^2-\sin^2\tau_j]^{\frac{1}{2}}\}/\{k_2^2\cos\tau_j/k_1^2+[k_2^2/k_1^2-\sin^2\tau_j]^{\frac{1}{2}}\}, \tag{27}$$

or for horizontal polarization,

$$R_m(\tau_j)=\{\cos\tau_j-[k_2^2/k_1^2-\sin^2\tau_j]^{\frac{1}{2}}\}/\{\cos\tau_j+[k_2^2/k_1^2-\sin^2\tau_j]^{\frac{1}{2}}\}, \tag{28}$$

where,

$$k_2=\frac{\omega}{c}\left[\epsilon_2-i\frac{\sigma\mu_0c^2}{\omega}\right]^{\frac{1}{2}} \tag{29}$$

and ϵ_2 is the dielectric constant of the earth ($\epsilon_2\sim15$) and σ is the conductivity of the earth ($\sigma\sim0.005$ for land). Since the examples considered in this paper involve distances which, for the first time-mode, were close to the geometric-optical horizon, it was found necessary to replace the Fresnel reflection coefficients with a more rigorous treatment.

Close to the geometric-optical horizon a calculation of $F_j=F_j^tF_j^r$ can be accomplished by a numerical evaluation of the contour integral, [Wait and Conda, 1958],

$$F_j^{t,r}\sim(\pi)^{-\frac{1}{2}}\exp[-ik_1a\theta']\int_{\infty\exp[-i2\pi/3]}^{\infty}\exp[-i(k_1a/2)^{\frac{1}{3}}\theta'\rho]/W_1'(\rho)-qW_1(\rho)\,d\rho, \tag{30}$$

$\theta'=(d-d_H)/a$, where d_H is the distance [3] from transmitter to the geometric-optical horizon ($\tau_j\sim\pi/2$) and,

$$q=-i\left(\frac{k_1a}{2}\right)^{\frac{1}{3}}\frac{k_1}{k_2}\sqrt{1-\frac{k_1^2}{k_2^2}}, \tag{31}$$

in which $\sigma=\sigma_2$ is the ground conductivity at either transmitter F_j^t or receiver F_j^r and ϵ_2 is the corresponding dielectric constants (relative to a vacuum), and,

$$W_1(\rho)=\exp[-2\pi i/3]\sqrt{\pi/3}\,(-\rho)^{\frac{1}{2}}H_{\frac{1}{3}}^{(2)}[2/3(-\rho)^{\frac{3}{2}}], \tag{32}$$

$$W_1'(\rho)=\exp[-2\pi i/3]\sqrt{\pi/3}\left\{-\frac{1}{2}(-\rho)^{-\frac{1}{2}}H_{\frac{1}{3}}^{(2)}\left[\frac{2}{3}(-\rho)^{\frac{3}{2}}\right]+\rho H_{\frac{1}{3}}'^{(2)}\left[\frac{2}{3}(-\rho)^{\frac{3}{2}}\right]\right\},$$

$$W_1'(\rho)=\exp[-i4\pi/3]\sqrt{\pi/3}\,\rho H_{\frac{1}{3}}^{(2)}\left[\frac{2}{3}(-\rho)^{\frac{3}{2}}\right] \tag{33}$$

$$H_{\frac{1}{3}}'^{(2)}(Z)=\frac{d}{dZ}H_{\frac{1}{3}}^{(2)}(Z)=\exp[-i2\pi/3]H_{\frac{1}{3}}^{(2)}(Z)-\frac{1}{3Z}H_{\frac{1}{3}}^{(2)}(Z). \tag{34}$$

The Hankel functions $H_{\frac{1}{3}}^{(1,2)}(Z)$ can be calculated by previously described quadrature methods (20–27). The contour integral can be written [Wait, 1960b],

$$F_j^{t,r}=(\pi)^{-\frac{1}{2}}\exp[-ik_1a\theta']\left\{\int_0^{\infty}\frac{\exp[-i(k_1a/2)^{\frac{1}{3}}\theta'\alpha]}{W_1'(\alpha)-qW_1(\alpha)}\,d\alpha-\int_0^{\infty}\frac{\exp[-i(k_1a/2)^{\frac{1}{3}}\theta'\alpha']}{W_1'(\alpha')-qW_1(\alpha')}\,d\alpha'\right\}, \tag{35}$$

$\alpha'=\alpha\exp(-i2\pi/3)$. These integrals can then be evaluated with a Gaussian quadrature.

Close to but beyond the geometric-optical horizon ($\tau_j\sim\pi/2$) [Wait and Conda, 1958], a calculation can be performed as a residue series summation,

$$F_j^{r,t}\sim-2i\sqrt{\pi}\exp[-ik_1(d-d_H)]\sum_{s=0}^{\infty}\frac{\exp[-i(k_1a)^{\frac{1}{3}}\theta'\tau_s^*]}{(2^{\frac{1}{3}}\tau_s^*-q^2)W_1(2^{\frac{1}{3}}\tau_s^*)} \tag{36}$$

[3] $a\sim6.367\,(10^6)$ m. In diffraction problems it is common practice to account for the vertical lapse of the permittivity of air at the earth's surface by use of an "effective earth radius", a_e, in place of a such that $\frac{a}{a_e}\sim0.75-0.85$, [Bremmer, 1949, p. 145].

where the complex conjugate τ_s of τ_s^* comprises the special roots of the differential equation of Riccati tabulated by Johler, Walters, and Lilley [1959], employing the time function, $\exp(-i\omega t)$,

$$\frac{d\delta_e}{d\tau_s}-2\tau_s\delta_e^2+1=0, \tag{37}$$

where

$$\delta_e=\frac{ik_2^2\alpha^{\frac{1}{3}}/k_1^2}{(k_1a)^{\frac{1}{3}}\left[\frac{k_2^2}{k_1^2}-1\right]^{\frac{1}{2}}}\sim i\frac{Z_0}{(k_1a)^{\frac{1}{3}}\left[\frac{-i\mu_0\omega}{\sigma-i\omega\epsilon}\right]^{\frac{1}{2}}} \tag{38}$$

and, $k_1=\frac{\omega}{c}\eta_1\sim\frac{\omega}{c}$, k_2^*, implies the complex conjugate of k_2, (3), and the limiting roots are found from the equations,

$$H_{\frac{2}{3}}^{(1)}\left[\frac{1}{3}(-2\tau_s)^{\frac{3}{2}}\right]=0,\ \delta_e=\infty,$$

$$H_{\frac{1}{3}}^{(1)}\left[\frac{1}{3}(-2\tau_s)^{\frac{3}{2}}\right]=0,\ \delta_e=0,$$

$$s=0,\ 1,\ 2,\ 3\ \ldots\ .$$

Finally, the effective reflection coefficient of geometric-optics, C_j, can be evaluated for vertical polarization,

$$C_j=\frac{1}{j!R_e}\frac{d^j}{dx^j}\left[\frac{1+A_1x}{1-A_2x-A_3x^2}\right]_{x=0}, \tag{39}$$

where,

$$A_1=-R_mT_{mm}$$

$$A_2=R_eT_{ee}+R_mT_{mm}$$

$$A_3=R_eR_m[-T_{ee}T_{mm}+T_{em}T_{me}]. \tag{40}$$

Thus, the essential nature of the propagation about the earth via the ionosphere can be described in terms of four reflection coefficients, T_{ee}, T_{em}, T_{me}, and T_{mm}. The reflection coefficient, T_{ee}, refers to the vertical electric polarization of the incident plane wave and a similar vertical electric polarization of the reflected wave. The coefficient, T_{em}, describes the generation of the abnormal component by the incident vertical polarization (reflected horizontal polarization for vertical excitation). Similarly, T_{mm} refers to the incident horizontal electric polarization and the corresponding reflected horizontal electric polarization. Also, the abnormal component generated by the horizontal electric polarization (reflected vertical polarization for horizontal excitation) is described by the coefficient, T_{me}. Thus, figure 3,

$$T_{ee}=E'_{y'r}/E_{y'i},\ T_{mm}=E_{x'r}/E_{x'i},\ T_{em}=E_{x'r}/E_{y'i},\ T_{me}=E_{y'r}/E_{x'i} \tag{41}$$

where the subscripts i and r refer to incident and reflected wave respectively at the ionosphere boundary. The calculation of these reflection coefficients has been previously described in detail and the results of various computations have been tabulated [Johler and Walters, 1960].

The reflection coefficients are completely specified by the angle of incidence, ϕ_i, figures 2, 3, electron density N(El/cm^3), figure 4, collision frequency ν(c/s), figure 5, magnetic field intensity H_m (gauss), magnetic dip I and magnetic azimuth ϕ_a. The effective reflection coefficients, C_j, can then be written in terms of the ionosphere reflection coefficients, T, and the ground reflection coefficients, R, for each local ionosphere or ground reflection,

$$C_1=C_1(\tau_1)=T_{ee},$$

$$C_2=C_2(\tau_2)=T_{ee_1}T_{ee_2}R_{e_1}+R_{m_1}T_{em_1}T_{me_2},$$

$$C_3=C_3(\tau_3)=R_{e_2}R_{m_1}T_{ee_3}T_{em_1}T_{me_2}+R_{e_1}R_{m_2}T_{ee_1}T_{em_1}T_{me_3}+R_{e_1}R_{e_2}T_{ee_1}T_{ee_2}T_{ee_3}+R_{m_1}R_{m_2}T_{mm_2}T_{em_1}T_{me_3}, \tag{42}$$

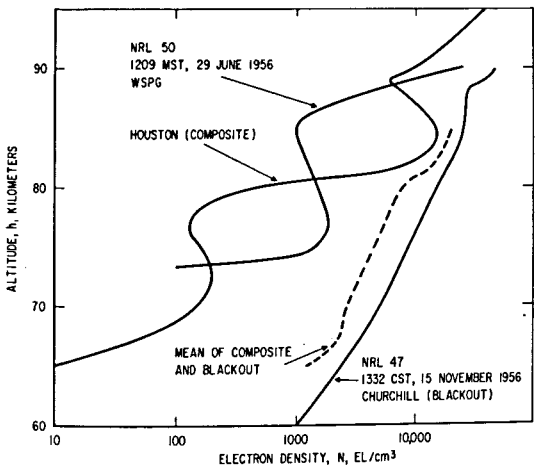

FIGURE 4. *Electron density-altitude,* N(h), *profiles of the lower ionosphere deduced from various radio and rocket measurements.*

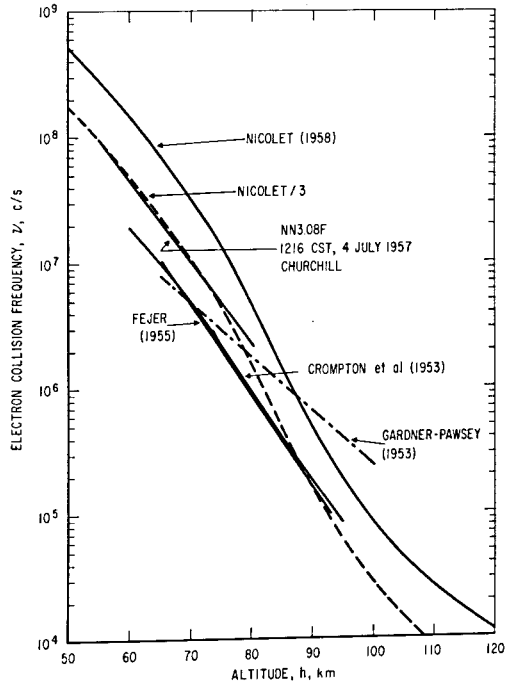

FIGURE 5. *Collision frequency-altitude,* ν(h), *profiles of the lower ionosphere deduced from theory and various rocket measurements.*

$$C_4=C_4(\tau_4)=R_{e_1}R_{e_2}R_{e_3}T_{ee_4}T_{ee_3}T_{ee_2}T_{ee_1}+R_{e_1}R_{e_2}R_{m_3}T_{me_4}T_{em_3}T_{ee_2}T_{ee_1}+R_{e_1}R_{m_2}R_{e_3}T_{ee_4}T_{me_3}T_{em_2}T_{ee_1}$$
$$+R_{e_1}R_{m_2}R_{m_3}T_{me_4}T_{mm_3}T_{em_2}T_{ee_1}+R_{m_1}R_{e_2}R_{e_3}T_{ee_4}T_{ee_3}T_{me_2}T_{em_1}+R_{m_1}R_{e_2}R_{m_3}T_{me_4}T_{em_3}T_{me_2}T_{em_1}$$
$$+R_{m_1}R_{m_2}R_{e_3}T_{ee_4}T_{me_3}T_{mm_2}T_{em_1}+R_{m_1}R_{m_2}R_{m_3}T_{me_4}T_{mm_3}T_{mm_2}T_{em_1}, \tag{43}$$

where the subscripts 1, 2, 3, 4 . . . refer to the first, second, third, fourth, etc., reflection regions of the ionosphere with corresponding separate values for electron density, N, collision frequency, ν, and the intensity and direction of the earth's magnetic field vector, $\overline{H}_m$, or, for the ground, refer to the separate values of conductivity, σ, and dielectric constant, ϵ_2.

For a homogeneous ionosphere and ground with a single set of values, N, ν, $\overline{H}_m$, σ, and ϵ_2, the effective reflection coefficients, C_j, reduce as follows:

$$C_1=T_{ee}$$
$$C_2=T_{ee}^2R_e+R_mT_{em}T_{me}$$
$$C_3=2R_eR_mT_{ee}T_{em}T_{me}+R_e^2T_{ee}^3+R_m^2T_{mm}T_{em}T_{me},$$
$$C_4=R_eR_m^2T_{em}^2T_{me}^2+3R_e^2R_mT_{ee}^2T_{em}T_{me}+2R_eR_m^2T_{ee}T_{mm}T_{em}T_{me}+R_m^3T_{mm}^2T_{em}T_{me}+R_e^3T_{ee}^4, \tag{44}$$
$$\ldots .$$

The wave number of the ionosphere propagation medium,

$$k_3=\frac{\omega}{c}\eta_0,$$
$$=\frac{\omega}{c}\eta_e, \tag{45}$$

implies two upgoing waves excited in the model ionosphere with index of refraction, η_0, for

595362—61——7

the "ordinary" wave and index of refraction, η_e, for the "extraordinary" wave. The value of the reflection coefficients, T, are related to the η_0 and η_e.

The rate of attenuation and phase lag of the wave, $\bar{E}_t$, transmitted into the ionosphere can be deduced by an interpretation of the transmitted wave in terms of the complex index of refraction, $\eta = \eta_{0,e}$.

$$E_t = |\bar{E}_t| \exp\left\{ i\left[\omega t - \frac{\omega}{c}\eta D\right]\right\}. \tag{46}$$

The amplitude is as follows:

$$\exp\left\{\frac{\omega}{c}\operatorname{Im}\eta D\right\}, \exp\{\text{nepers}\}, \tag{47}$$

or the amplitude change is,

$$\exp\left\{\frac{\omega}{c}\operatorname{Im}\eta\, 10^3\right\}, \exp\{\text{nepers/km}\}, \tag{48}$$

$$\text{or, } 8.686\frac{\omega}{c}\operatorname{Im}\eta D, \text{ decibels}, \tag{49}$$

$$\text{or, } 8.686\frac{\omega}{c}\operatorname{Im}\eta\, 10^3, \text{ db/km}, \tag{50}$$

where D (meters) is the penetration distance into the ionosphere. The corresponding phase lag is,

$$\frac{\omega}{c}\operatorname{Re}\eta D \text{ radians}, \tag{51}$$

or,

$$\frac{\omega}{c}\operatorname{Re}\eta(10^3) \text{ radians/km}. \tag{52}$$

3. Analysis of Experimental Data

Although there is a tendency in LF propagation studies to separate arctic-auroral phenomena from those phenomena observed at LF in temperate latitudes, the mechanism of propagation seems to differ only in the degree and frequency of the so-called disturbed and blackout conditions which characterize the arctic regions. Certain data on propagation at LF in both the arctic-auroral regions and the temperate regions are analyzed in this paper to demonstrate principle rather than deduce comprehensive engineering conclusions. A theoretical investigation and analysis is therefore attempted to gain some insight into LF propagation phenomena for Loran-C system evaluation.

Ionosphere electron density-altitude profiles $N(h)$, figure 4, and collision frequency-altitude profiles $\nu(h)$, figure 5, have recently been deduced with the aid of a theoretical method and an experimental HF signal transmitted through the ionosphere from rockets. Waynick [1957] reported the "Houston composite," figure 4 $N(h)$ profile, and Seddon and Jackson [1958] have reported "NRL 50" and "NRL 47" profiles. Seddon and Jackson have also reported "NN3.08F" $\nu(h)$ profile, figure 5. Other $\nu(h)$ data are shown from Crompton et al. [1953], Gardner and Pawsey [1953], Fejer [1955], and Nicolet [1958].

The "Houston composite" $N(h)$ profile implies an interesting low electron density region at the 65 to 70 km altitudes of the lower ionosphere with values between $N=10$ and $N=100$ El/cm^3, figure 4. Such a profile seemed to persist in the propagation data examined and profoundly influenced the daytime ionospheric propagation. However, it does not appear to exist in the "NRL 50" data which seems to give rise to great electron densities quite abruptly. Unfortunately, as a result of rocket drag considerations, the HF antennas were not extended until the rocket attained an altitude of about 55 km, and measurements of electron densities in this region are not very detailed. This lack of data below 60 km is more apparent in the "NRL 47" data, observed in the auroral zone at Churchill, Canada, which illustrate a very large enhancement of the electron density during auroral "blackout" conditions. A "mean of the

composite and blackout" profiles was employed as an intermediate "disturbed" model ionosphere.

Various collision frequency-altitude profiles, $\nu(h)$, are shown in figure 5. The "Nicolet/3" curve was used for all model ionospheres employed in this analysis. This is a theoretical curve substantiated with experimental rocket data. This theoretical curve is also consistent with other findings [Ratcliffe, 1959].

Theoretical field intensities, figures 6 to 9, were calculated for comparison with available data[4] on LF transmission from Adak to Nome and Kodiak, Alaska. The independent variable

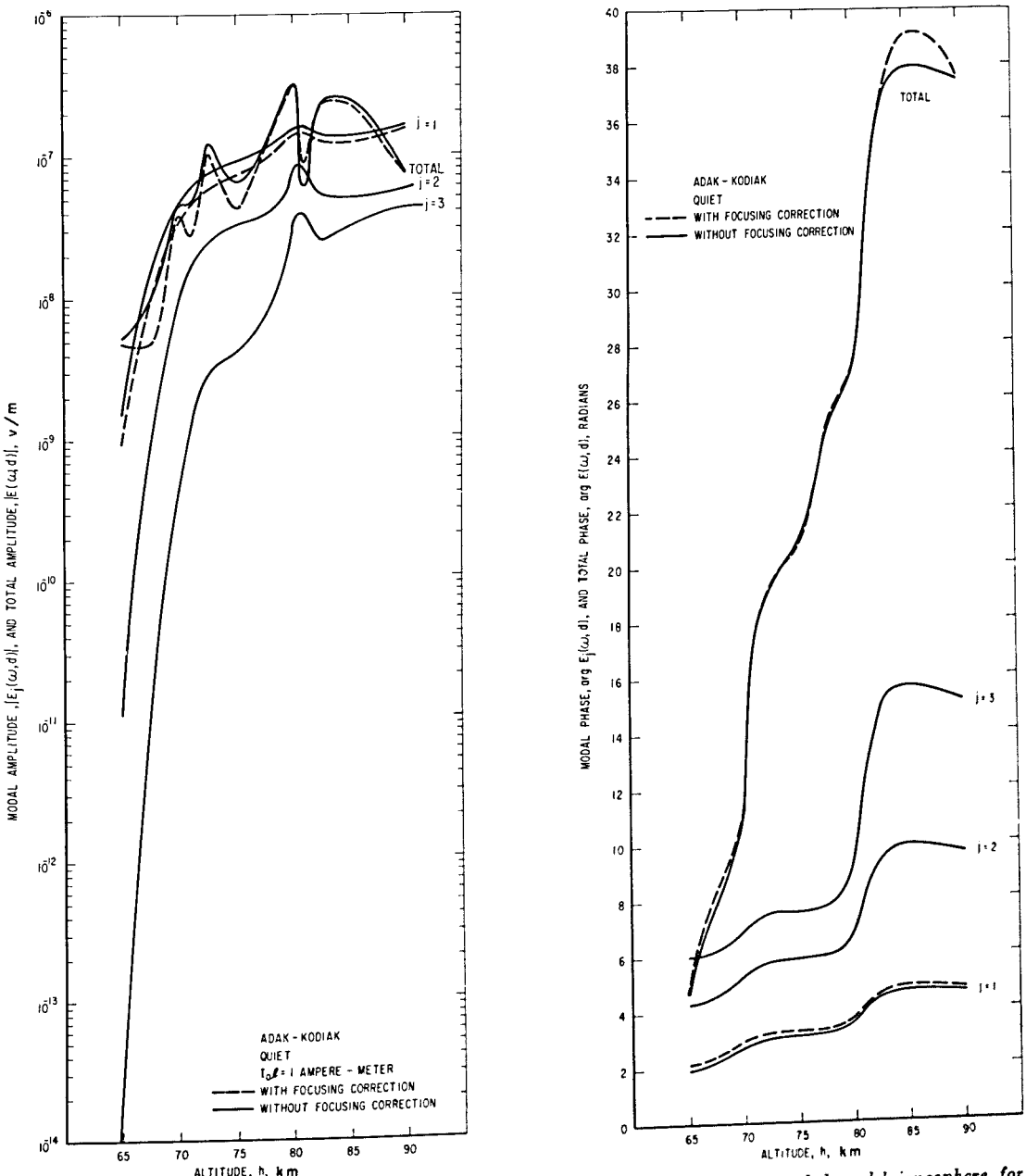

FIGURE 6. *Total theoretical field* E(ω, d) *for various fixed heights,* h, *of sharply bounded model ionosphere for LF transmissions from Adak to Kodiak, Alaska.*

(See figures 4 and 5 for electron density N . . . .)

[4] The data employed in this analysis is treated somewhat differently from previous authors. The authors wish to thank A. D. Watt and J. E. Bickel for the use of their original data. See also Bickel [1959] and Watt et al. [1959].

of the calculations was the altitude, h, of the assumed sharply bounded model ionosphere. This implies a variation of the electron density according to the $N(h)$ profile as the variable h is changed. Also, small adjustments in the angle of incidence, ϕ_i, are implied.

Geophysical data on the ionosphere employed in the calculation are shown, tables 1, 2. The magnetic data, shown in table 2, were scaled from Magnetic Charts [1954, 1957]. Apparently a nominal intensity value $H_m=0.5$ gauss (table 2) is an adequate assumption for many practical cases.

TABLE 1

h	ν	N_q	N_d	N_b
km	*c/s*, $\times 10^{+6}$	El/*cm*^{3}	El/*cm*^{3}	El/*cm*^{3}
55	175			10
60	50			1000
65	24	10	1205	2400
67.5	16	56		
70	10.9	150	2675	5200
71	9.2	180		
72.5	7	200		
75	4.5	160	4505	8850
77.5	2.6	140		
80	1.6	500	7950	15400
81	1.2	3500	10550	
82.5	0.88	11000	16100	
85	.465	15000	20500	26000
90	.155	10000		

TABLE 2.—*Magnetic field, $\overline{H}_m$, data*

	Reflection number	H_m	I	ϕ_a
Adak-Nome, d=965.5 statute miles (1,550 *km*)				
		Gauss	*deg*	*deg*
1	1st	0.5187	68.68	12.27
2	1st	.4996	65.75	12.52
2	2d	.5329	71.52	11.72
2	1st	.4952	64.82	12.63
3	2d	.5187	68.68	12.27
3	3d	.5388	72.46	11.66
Adak-Kodiak, d=1040.1 statute miles (1,670 *km*)				
1	1st	0.5035	67.18	51.08
2	1st	.4950	65.15	52.84
2	2d	.5170	69.04	49.73
3	1st	.4923	64.42	53.42
3	2d	.5035	67.18	51.08
3	3d	.5262	69.64	49.35

The modal (skywave time-mode) and the total (including the groundwave) calculated fields (amplitude and phase) for quiescent, disturbed, and blackout conditions of the ionosphere are presented, figures 6 to 9. The effect of the ionosphere focusing corrections, A_j, is also illustrated, and, indeed, was found to be appreciable, both for the total field, $E(\omega,d)$, and the first modal field, $E_j(\omega,d), j=1$. The diffraction correction F_j was also modified from the classical Fresnel reflection coefficient as discussed with the aid of calculated data of Wait and Conda [1958] which was installed in the electronic memory of a small computer.[5]

The ground wave, $E_0(\omega,d)$, which was calculated with the classical Bremmer-van der Pol theory [Johler, Kellar, and Walters, 1956] and corrected for land-sea boundaries with the aid of the Millington [1949] method is not shown alone graphically, since the groundwave is not a function of the emplacement altitude, h, but can be summarized as follows:

TABLE 3

	$E_0(\omega,d)$		arg $E_0(\omega,d)$
	I_0l=1	I_0l=2050	
	v/m	*v/m*	*Radians*
Nome	7.56(10^{-9})	1.55(10^{-5})	2.30
Kodiak	4.64(10^{-9})	9.51(10^{-6})	2.43

[5] IBM-650.

All computations were made with the assumption of a dipole current moment, $I_0l=1$. The total radiated power, $Pr=1.3$ kw, for the arctic data considered was found to correspond to a dipole current moment, $I_0l=2050$ amp-m; therefore, the calculated field amplitude, $[E(\omega,d)]$, or $[E_j(\omega,d)]$, has been increased by this factor for comparison with the data.

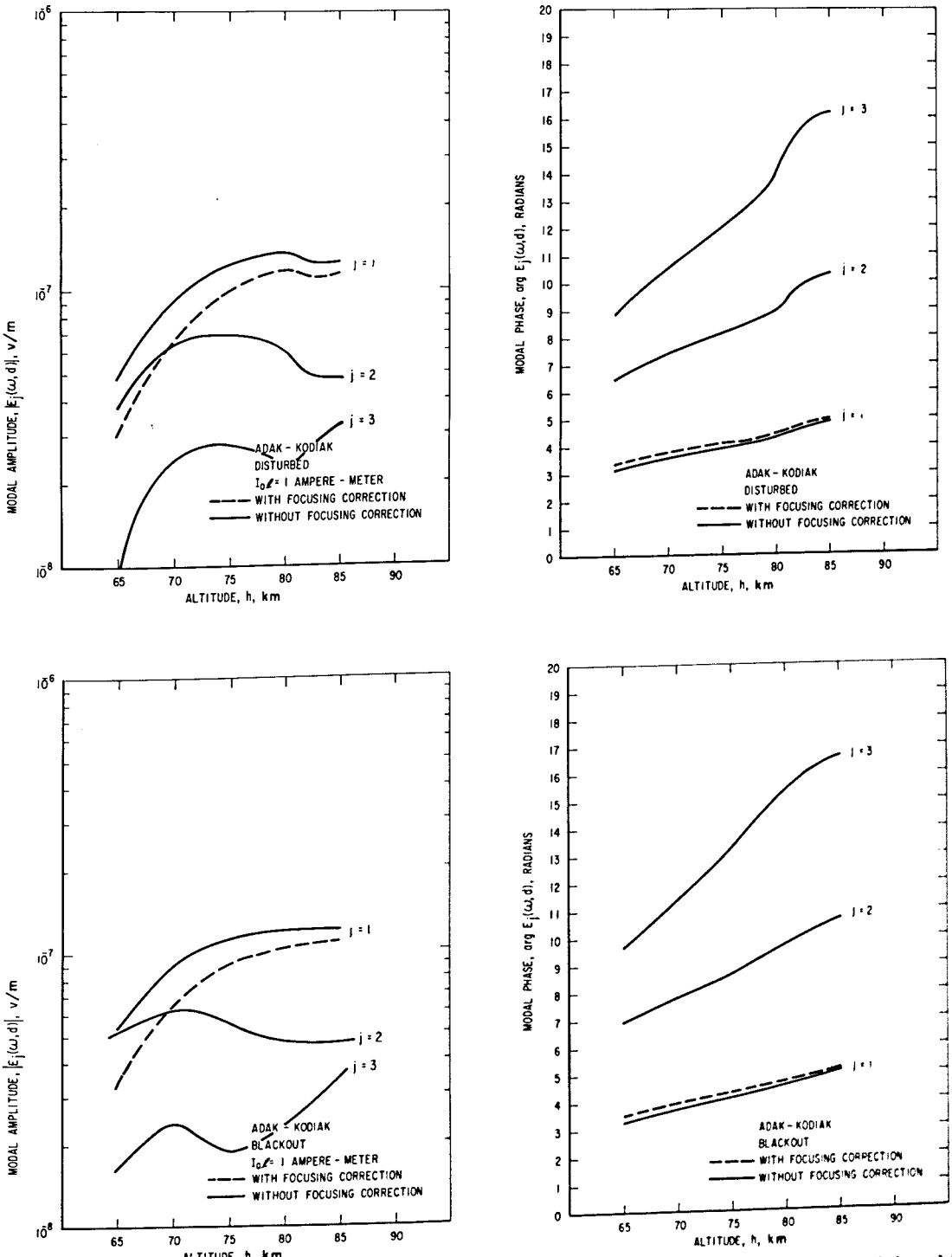

FIGURE 7. *Disturbed-blackout theoretical field* $E(\omega, d)$ *for various fixed heights, h, of sharply bounded model ionosphere for LF transmissions from Adak to Kodiak, Alaska.*

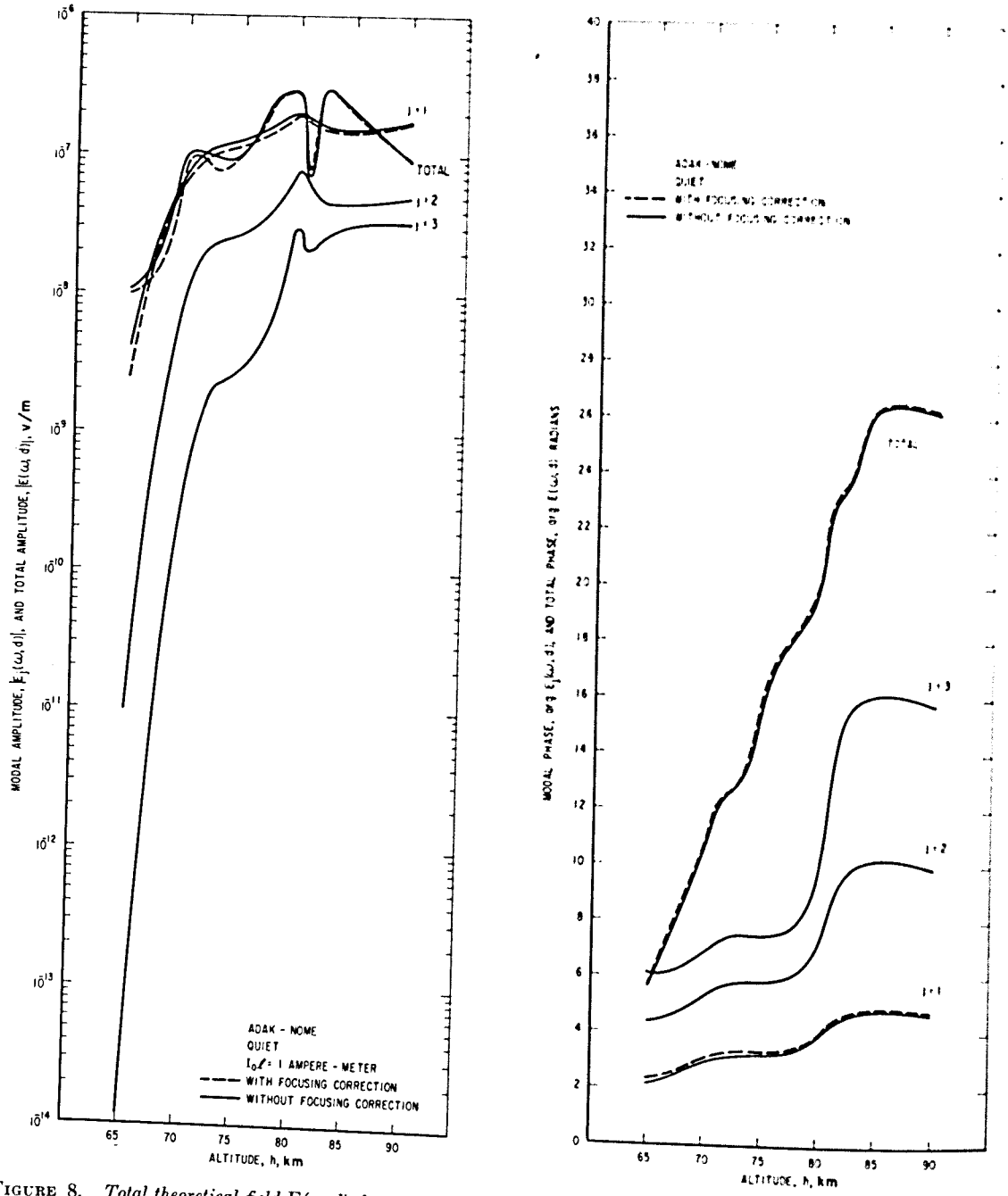

FIGURE 8. *Total theoretical field* $E(\omega, d)$ *for various fixed heights,* h, *of sharply bounded model ionosphere for LF transmissions from Adak to Kodiak, Alaska.*

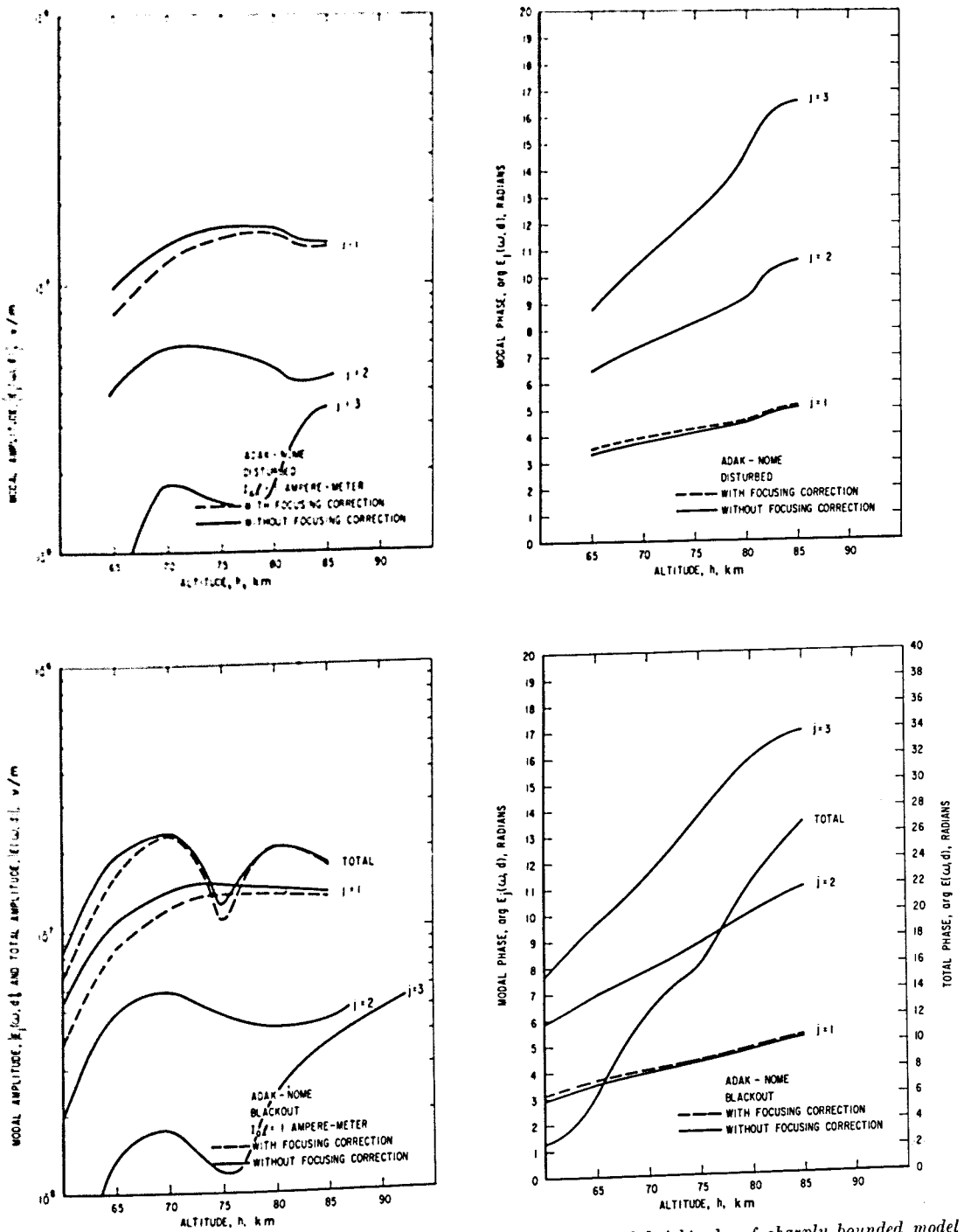

FIGURE 9. *Disturbed-blackout theoretical field* $E(\omega, d)$ *for various fixed heights,* h, *of sharply bounded model ionosphere for LF transmissions from Adak to Kodiak, Alaska.*

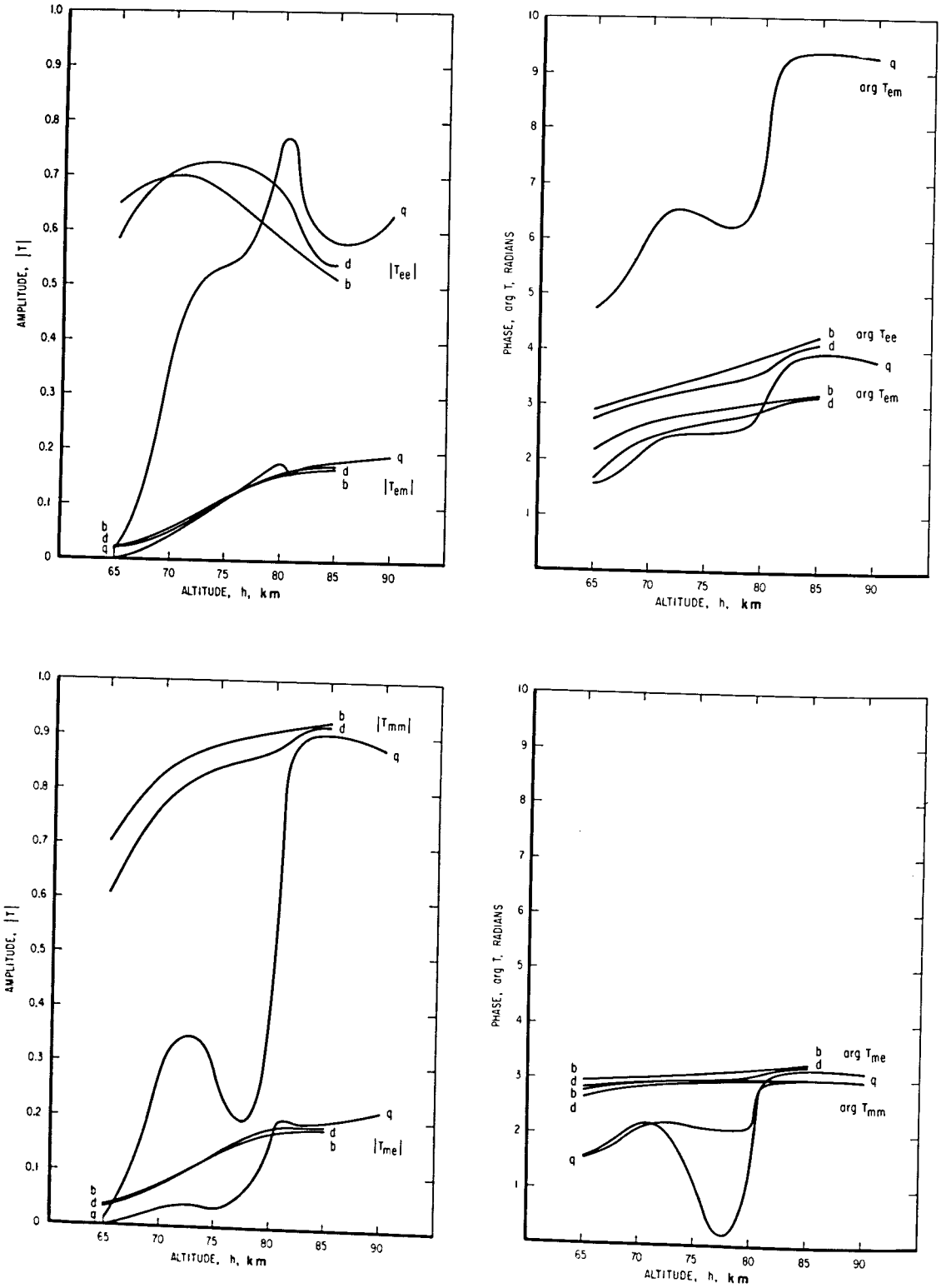

FIGURE 10. *Comparison of quiescent and disturbed-blackout conditions of theoretical reflection coefficient,* T, (j=1), *for various fixed heights,* h, *of sharply bounded model ionosphere for LF transmissions from Adak to Kodiak, Alaska.*

H_m=0.5035, ϕ_s=51.08°, I=67.18°

In addition to the total field, $E(\omega,d)$, and the modal field, $E_j(\omega,d)$, figures 6 to 9, the reflection coefficients, T, (horizontal and vertical polarization; normal and abnormal components), figures 10 to 11, and the transmission data of the ordinary and extraordinary upgoing

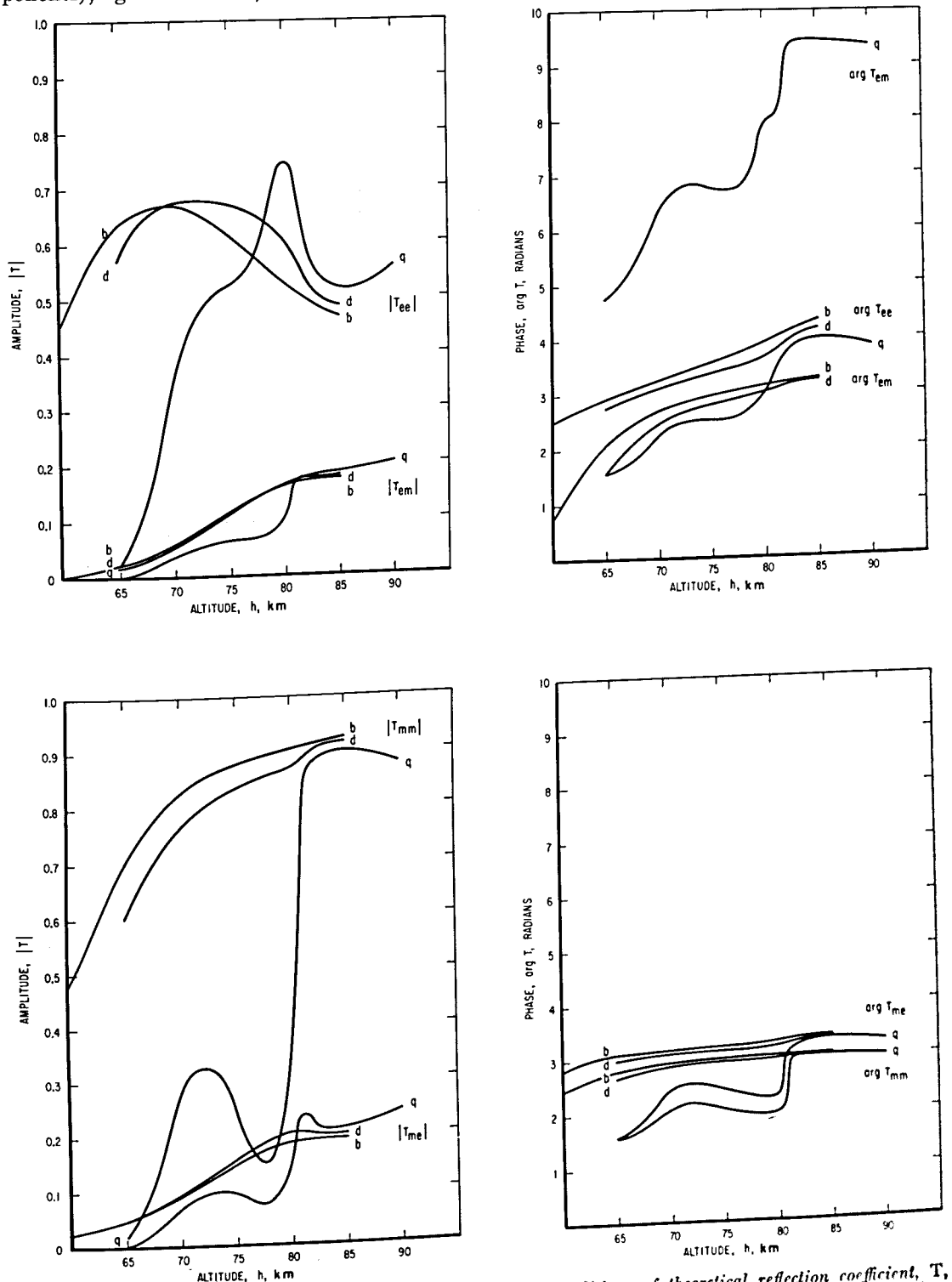

FIGURE 11. *Comparison of quiescent and disturbed-blackout conditions of theoretical reflection coefficient,* T, (j=1), *for various fixed heights,* h, *of sharply bounded model ionosphere for LF transmissions from Adak to Nome, Alaska.*
H_m=0.5187, ϕ_a=12.27°, I=68.68°.

595362—61——8

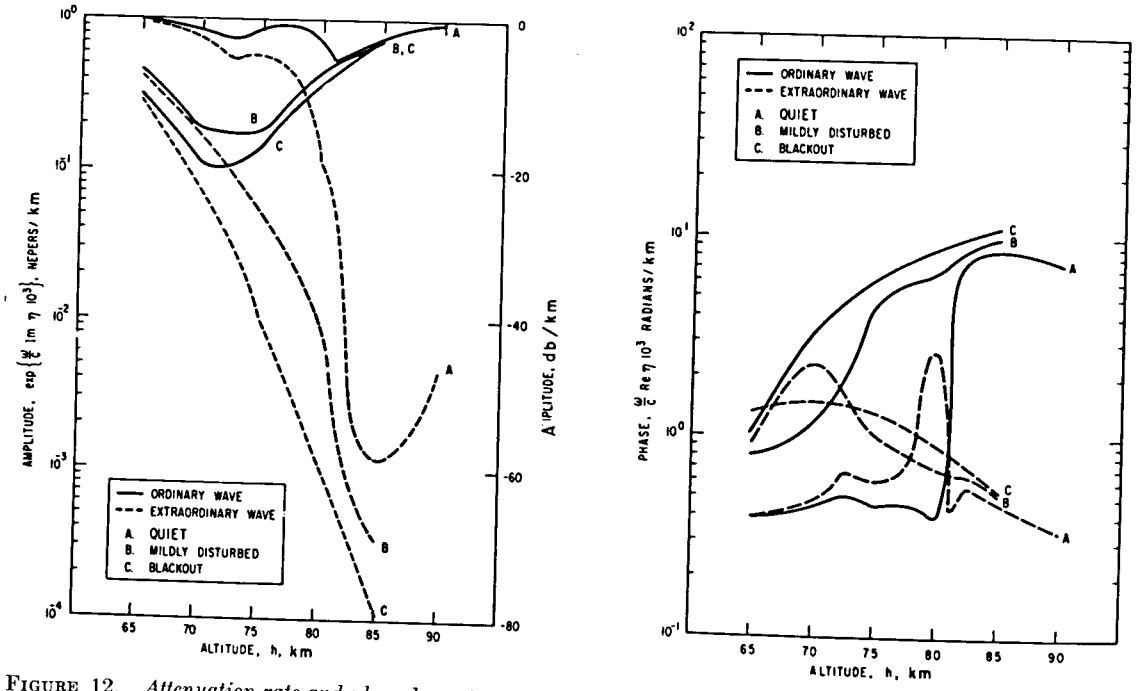

FIGURE 12. *Attenuation rate and phase lag rate at various emplacement altitudes, h, for upgoing "ordinary" and "extraordinary" waves excited in the model ionosphere by Adak to Kodiak, Alaska transmissions during quiescent and disturbed-blackout conditions.*

First time-mode: $H_m=0.5035$, $\phi_a=51.08°$, $I=67.18°$.

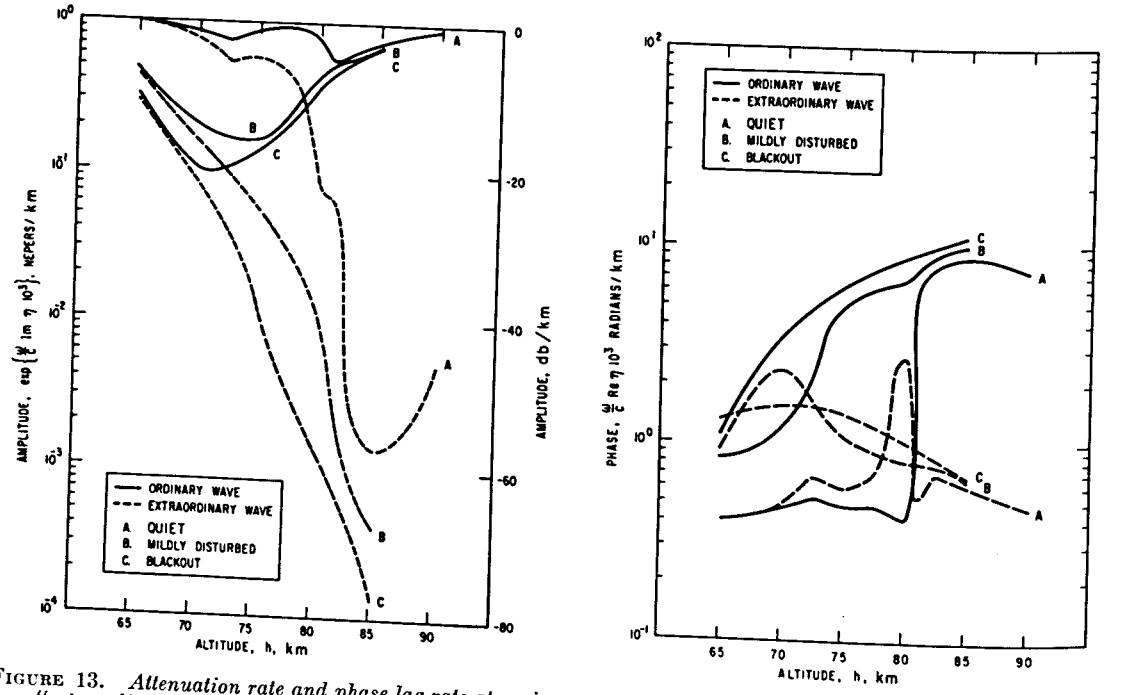

FIGURE 13. *Attenuation rate and phase lag rate at various emplacement altitudes, h, for upgoing "ordinary" and "extraordinary" waves excited in the model ionosphere by Adak to Nome, Alaska transmissions during quiescent and disturbed-blackout conditions.*

First time-mode: $H_m=0.5187$, $\phi_a=12.27°$, $I=68.68°$.

waves excited in the ionosphere by the reflection process, figures 12, 13, were evaluated. The unabsorbed modal field, $E_j(\omega,d)/C_j$, and the effective reflection coefficients, C_j, are separately illustrated, figures 14 and 15, respectively.

The emplacement height, h, of the model ionosphere was deduced by comparison of the computed field strength, $E(\omega,d)$, with the measured value. The corresponding four reflection coefficients, T_{ee}, T_{em}, T_{mm}, T_{me}, (amplitude and phase) were then evaluated from the theory. The results of this process which were readily scaled from graphs such as illustrated, figures 10, 11, are presented in table 4, and the reflection coefficients deduced for the first time-mode only are presented.

The higher order time-mode, $j=2$, 3, reflection coefficients are obviously quite numerous since a separate set exists for each ionosphere reflecting region. These reflection coefficients are determined by the analysis by reference to the emplacement altitude, h, table 5, deduced from the field, $E(\omega,d)$.

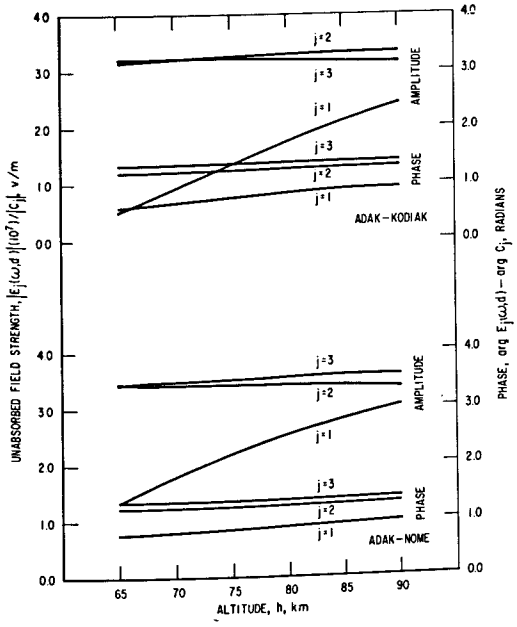

FIGURE 14. *Unabsorbed modal field,* $E_j(\omega, d)/c$, *at various model ionosphere altitude emplacements,* h, *for Adak to Nome and Kodiak, Alaska transmissions* $I_0l=1$ *ampere-meter.*

TABLE 4

% Time Field $\|E\|$ exceeded	Season and year	Observed $\|E(\omega, d)\|$	h	arg $E(\omega,d)$	$\|E_1(\omega, d)\|$	arg $E_1(\omega, d)$	$\|T_{ee}\|$	arg T_{ee}	$\|T_{em}\|$	arg T_{em}	$\|T_{mm}\|$	arg T_{mm}	$\|T_{me}\|$	arg T_{me}
Adak-Kodiak (Daytime)														
		μv/m	*km*	*Radians*	*μv/m*	*Radians*								
10	Winter 1953-54	33	69	10.4	56	2.8	0.27	2.1	0.03	5.8	0.23	2.0	0.03	2.1
50		12	68	9.5	35	2.6	.19	2.0	.02	5.7	.16	1.9	.02	2.0
90		4.8	<65	<5.0	<2.0	<2.1	<.02	<1.6	0	<4.8	<.02	<1.6	0	<1.6
10	Autumn 1954	20	69	10.4	56	2.8	.27	2.1	.03	5.8	.23	2.0	.03	2.1
50		7.1	<65	<5.0	<2.0	<2.1	<.02	<1.6	0	<4.8	<.02	<1.6	0	<1.6
90		2.6	<65	<5.0	<2.0	<2.1	<.02	<1.6	0	<4.8	<.02	<1.6	0	<1.6
Adak-Nome (Daytime)														
10	Winter 1953-54	124	69	9.8	94	3.0	0.29	2.1	0.03	5.95	0.23	1.95	0.055	2.25
50		56	68	9.0	60	2.7	.18	1.9	.02	5.55	.15	1.8	.04	2.0
90		22	65.5	6.4	9.0	2.4	.04	1.6	.01	4.8	.035	1.6	<.01	1.6
10	Autumn 1954	64	68.5	9.3	70	2.8	.22	1.95	.025	5.7	.18	1.9	.045	2.1
50		28	66.5	7.4	22	2.5	.08	1.65	.01	5.0	.065	1.65	.015	1.75
90		11	<65	<5.7	<5.0	<2.3	<.02	<1.55	0	<4.75	<.02	<1.6	0	<1.6
10	Spring 1954	34	67	7.8	36	2.6	.11	1.75	.015	5.2	.09	1.7	.02	1.8
50		19	<65	<5.7	<5.0	<2.3	<.02	<1.55	0	<4.75	<.02	<1.6	0	<1.6
90		10	<65	<5.7	<5.0	<2.3	<.02	<1.55	0	<4.75	<.02	<1.6	0	<1.6

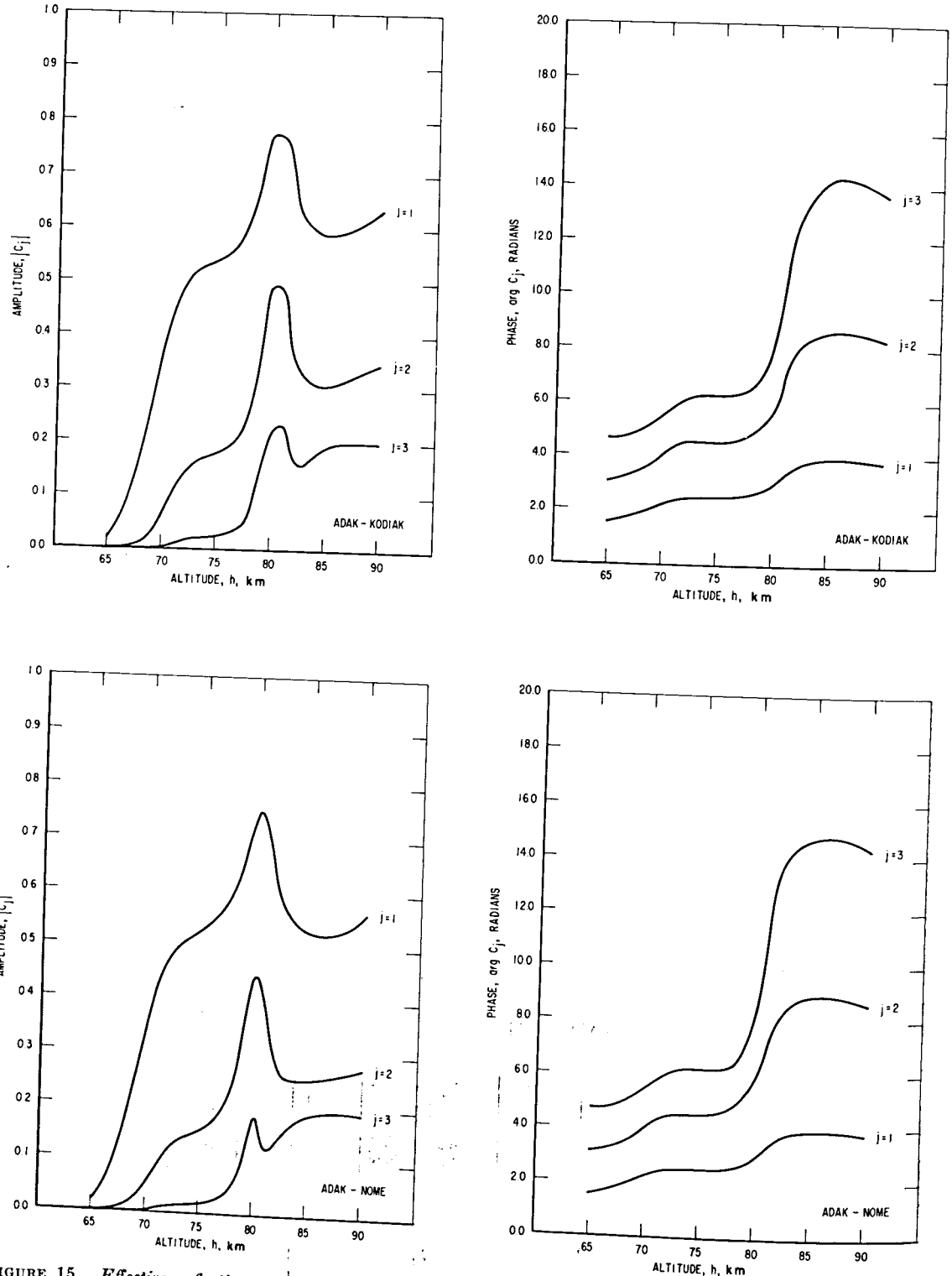

FIGURE 15. *Effective reflection coefficient,* c_j, *for Adak to Nome and Kodiak, Alaska, transmissions under quiescent ionosphere conditions.*

TABLE 5

Condition	Mode	N	h	$\lvert E(\omega,d)\rvert$	arg E
		El/cm³	*km*	*v/m*	*radians*
b	Total	10	55	7.59 (10^{-9})	5.54
b	Total	1000	60	6.60 (10^{-8})	2.84
b	$j=1$	10	55	1.18 (10^{-10})	2.10
q	Total	10	65	9.77 (10^{-9})	5.66
q	$j=1$	10	65	2.42 (10^{-9})	2.33

It is interesting to note emplacement altitudes, h, less than 65 km under quiescent conditions. Indeed, the highest altitude for these daytime values was 69 km (winter 1954). A good nominal daytime emplacement altitude is 67.5 km. The low value ($|T|<0.1$) reflection coefficients are also quite interesting. Note the highest value, $|T|\sim0.27$. Note also, the median value at Nome (1954 equinox), $|T_{ee}|=0.08$. A low value $|T|<0.1$, and "black", $|T|\sim0$ appearance of the ionosphere indicates a low level absorbing region in the lower ionosphere at grazing incidence. A region of low electron density, $N=10$–100 El/cm³, is indicated by the model employed, figure 4. The transmission into such a region at grazing incidence, $\phi_i\sim80°$, figures 11, 12, indicates almost complete absorption of both the "ordinary" and the "extraordinary" rays if a "virtual height," $h+\Delta h$, is assumed of the order of 70 km. The transmission curves, figures 11, 12, demonstrate that the "extraordinary" ray is very highly attenuated such that it is necessary to consider only the "ordinary" ray. Assuming 1 db/km, for example, figures 11, 12, and a virtual height, $h+\Delta h$, of 70 km, noting that appreciable attenuation rate begins at 65 km, the total attenuation can be estimated; total decibels$\sim2\Delta h/\cos\phi_i\sim57$ db. This, of course, neglects a reflection absorption at the 70 km virtual height plus the transmission absorption back into the region below the ionosphere. The values, Δh, can be decreased and a corresponding decrease in the attenuation noted. But a repetition of the process leads to the interesting conclusion that most of the ray reflection must occur in a fraction of a kilometer, and, hence, the sharply bounded model can be reasonably applied under these conditions to predict the LF field, $E(\omega,d)$. A similar examination of the second and third time-modes leads to an almost similar reflecting region since the angle of incidence, ϕ_i, figure 2, does not change rapidly until the distance, d/j, is sufficiently short. It is, nevertheless, conceivable that the amplitude of the skywave reflections, $j=4, 5, 6, \ldots$ at shorter distances could become quite large as a result of reflection from a high level "virtual height," $h+\Delta h=70$ to 85 km. Under these conditions, however, the sharply bounded model would not be valid and it would be necessary to develop theoretical techniques for a diffusely bounded model ionosphere.

Information on the lower ionosphere $N(h)$ profile during nighttime conditions is quite sparse and hence the theoretician can only speculate on its nature. However, under certain reasonable assumptions, a possible explanation of the increase in field strength experienced at night may be deduced from the daytime model ionosphere employed.

Despite the seeming "evaporation" of the lower regions of the ionosphere at night with a corresponding abrupt increase of the electron density to a large finite value, it seems reasonable to assume that this abrupt increase does not occur within $\lambda/10$ or 0.22 km at 135.6 kc/s. This makes it possible to utilize the present sharply bounded model ionosphere, if it is emplaced at a higher level. Recent work [Ellyett and Watts, 1959] indicates a height of 80 to 85 km is not unreasonable.

Since the change of the angle of incidence, ϕ_i, figure 2, with ionosphere height, h, is not great at this range, we may neglect its effect on the field strength, figures 6 to 9, and the effective reflection coefficients, figure 15. The only factor changed, therefore, is the unabsorbed field, figure 14. It therefore seems reasonable to expect the first time mode, $|E_1(\omega,d)|$, to increase on the order of at least twice, whereas, reference to the arctic data and figure 16, "Battle Lake data" (to be discussed below), indicates an increase of perhaps 4 to 10 times. This could easily be explained by a slight change of slope in the $N(h)$ profile employed as evidenced by the steep slope of the C_1 curves ($j=1$), figure 15, in the region involved. On this basis, it is reasonable to expect a nighttime reflection coefficient, $|T|\sim0.3$, 0.4. Indeed, at temperate latitude, these values are confirmed [Ross, 1959].

It is not surprising that a large phase change could be expected during the sunset-sunrise transition periods, figures 6 and 8. Indeed, such phase changes were described at 100 kc/s by Doherty [1957], while operating the Loran-C on the first time-mode of the skywave.

The behavior of the LF propagation during disturbed and blackout conditions which are especially frequent in the arctic-auroral region is not quite so clear. Figures 7 and 9 illustrate disturbed-blackout conditions based on the geophysical measurements of electron density profiles, $N(h)$, of the lower ionosphere, figure 4. The corresponding reflection coefficients, figures 10, 11, and the transmission of upgoing ordinary and extraordinary waves excited by the reflection process are also illustrated, figures 12, 13. The disturbance of the earth's magnetic field during extreme blackout conditions is negligible since the total field, $H_m \sim 0.5$ gauss and the fluctuations are of the order of 0.001 gauss [Chapman, 1940]. The most significant change in the propagation is caused by the drastic change in the electron density profile, $N(h)$, figure 4. Unfortunately, the shape of the lower levels, <60 km, of the "blackout" $N(h)$ profile is unknown. Since the analysis under quiescent conditions indicates low-electron density reflections, the curve, figure 4, was extrapolated, and the corresponding field, $E(\omega,d)$, calculated for Adak to Nome transmission. The results are tabulated in table 5.

Note the $j=1$ mode for a region of $N=10$ El/cm^3 has undergone a 26 db decrease and the total field is therefore almost entirely groundwave. Appreciable as the decrease is, it is still well within the range of observations of arctic data. Notice, figure 16 "Battle Lake data" (to be discussed below), that the range of observations in temperate latitudes is approximately 18 db. The additional fluctuation may then, reasonably, be attributed to the change in electron density of the extreme lower ionosphere. If this change were to be so abrupt as to reach $N=1000$ El/cm^3 in, say, $\lambda/10$ km, the field strength would show a considerable increase, instead of decrease. It is reasonable to expect that a more realistic value of somewhat less than $N=1000$ El/cm^2 would also produce an increase in the received field strength. The shape of the $N(h)$ profile, thus, becomes quite important.

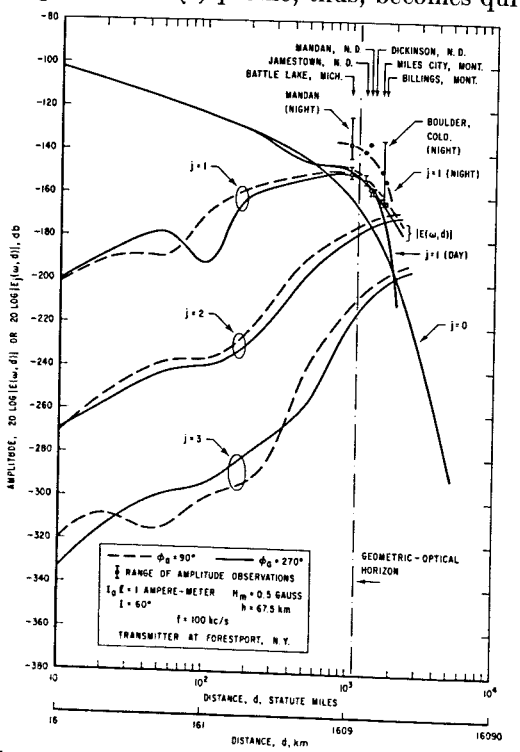

FIGURE 16. *Amplitude of theoretical total field* $|E(\omega, d)|$ *as a function of distance,* d, *from the source illustrating a comparison of experimental pulse amplitude measurements with theoretical first time-mode in the diffraction zone beyond the geometrical-optical horizon.*

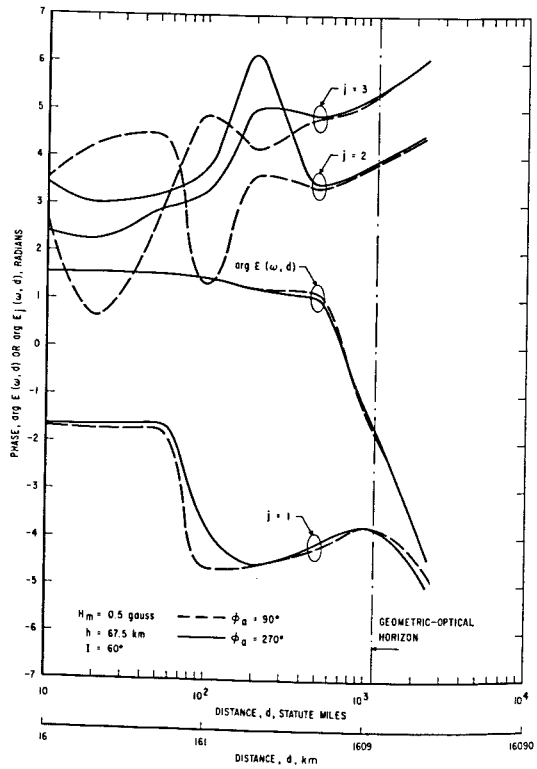

FIGURE 17. *Phase of theoretical field arg* $E(\omega, d)$ *as a function of distance.*

The calculation of the amplitude and phase of the total field, $E(\omega,d)$ as a function of distance is illustrated in figures 16 and 17. The corresponding reflection coefficient T_{ee} (vertical polarization, normal component) is illustrated in figure 18.

Amplitude measurements [6] during the day which illustrate the diffraction of the first time-mode ($j=1$) near and beyond the geometric-optical horizon are illustrated in figure 16. The agreement with the theoretical curve $j=1$ appears to be quite close except at the range of 1,800 miles. It is interesting to note the apparent decrease in the range of amplitude observations in the daytime, indicating greater amplitude stability with range in the diffraction zone.

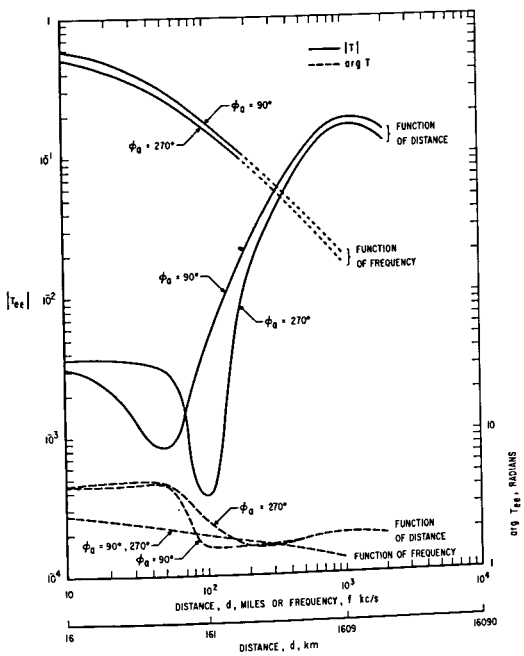

FIGURE 18. *Amplitude and phase of the normal component reflection coefficient* T_{ee} *(vertical polarization) as a function of distance and frequency for east-to-west* $\phi_a=270°$ *and west-to-east* $\phi_a=90°$ *propagation.*

4. Conclusion

The analysis of these data demonstrates the application of propagation theory together with a suitable model for the ionosphere to the prediction of LF phenomena. The precision of the model for the case of transmission via the ionosphere at or close to grazing incidence is considered to be adequate upon considering the state of knowledge of the many parameters which influence such propagation. Nevertheless, the absence of an abundance of specific information does not deter the author from certain general conclusions which can be made as a result of this research.

At oblique incidence on the ionosphere, a condition which is certainly met under most practical situations, the reflection of LF waves during the daytime occurs in a region of very low electron density and high absorption, with corresponding low values of reflection coefficients, $|T|<0.1$. The dominant skywave time-mode is, in general, the first; however, the second, third and higher order time-modes may offer appreciable contribution to the total field as the angle of incidence decreases as a result of reflection from higher levels and shorter transit distance in the ionized medium.

Periods of ionospheric disturbance (blackout) can produce a decrease in the field as a result of a reduction in the amplitude of the ionospheric time-modes. However, it is equally possible for the skywave mode to be incremented. This phenomenon is dependent upon the slope of

[6] From the author's personal notes on the 1953–1954 testing of the Loran-C (Cytac) System.

the electron density-altitude profile, $N(h)$ h. However, if ordinary communication is an engineering objective, LF seem to be quite reliable since the characteristic high absorption of HF waves does not appear to exist.

Since the writing of this paper the extensive theoretical work of Barron [1961] and the extensive experimental and engineering work of Belrose et al., [1959] have come to the attention of the author. It is interesting to note quite good agreement, figure 18, between the reflection coefficients deduced from the sharply bounded model presented in this paper and those presented as a result of Barron's full wave computations. Barron's data does, however, indicate, as might be expected, higher attenuation at the higher frequencies (>150 kc/s).

It should be noted in conclusion that the adequacy of the sharply bounded model is subject to severe limitations, especially at the higher frequencies and the results of this paper suggest also the introduction into this geometric optical analysis of more rigorous or flexible models for the reflection coefficient which would treat a more diffuse ionosphere lower boundary.

5. References

Ballantine, S., On the radiation resistance of a simple vertical antenna at wave lengths below the fundamental, Proc. IRE **12,** 823–829 (Dec. 1924).

Barron, D. W., The numerical solution of differential equations governing the reflexion of long radio waves from the ionosphere, IV, Proc. Roy. Soc. **260,** Ser. A, No. 302, 393–408 (March 1961).

Belrose, J. S., W. L. Hutton, C. A. McKerrow, and R. S. Thain, The engineering of communication systems for low radio frequencies, Proc. IRE **47,** No. 5, pt. 1, 661–680 (May 1959).

Bickel, J. E., A method for obtaining LF oblique incidence reflection coefficient and its application to 135.6 kc data in the Alaska area, J. Geophys. Research **62,** No. 3, 373–381 (Sept. 1957).

Bremmer, H., Terrestrial radio waves—theory of propagation (Elsevier Publishing Co., New York, N.Y., 1949).

Chapman, S., and J. Bartels, Geomagnetism, Vol. I (Oxford at the Clarendon Press, 1940).

Crompton, R. W., L. G. H. Huxley, and D. J. Sutton, Experimental studies of the motions of slow electrons in air with applications to the ionosphere, Proc. Roy. Soc. London **218,** Ser. A, 507–519 (July 1953).

Davis, P., and P. Rabinowitz, Abscissas and weights for Gaussian quadratures of high order, J. Research NBS **56,** 35–37 (Jan. 1956).

Doherty, R. H., private communication (1957).

Ellyett, C., and J. M. Watts, Stratification in the lower ionosphere, J. Research NBS **63D** (Radio Prop.). No. 2, 117–134 (Sept.–Oct. 1959).

Fejer, J. A., The interaction of pulsed radio waves in the ionosphere, J. Atmospheric and Terrest. Phys. **7,** 322–332 (Dec. 1955).

Gardner, F. F., and J. L. Pawsey, Study of the ionospheric *D*-region using partial reflections, J. Atmospheric and Terrest. Phys. **3,** 321–344 (July 1953).

Johler, J. R., Magneto-ionic propagation phenomena in low- and very low-radiofrequency waves reflected by the ionosphere, J. Research NBS **65D,** (Radio Prop.), No. 1, 53–61 (Jan.–Feb. 1961).

Johler, J. R., W. J. Kellar, and L. C. Walters, Phase of the low radiofrequency ground wave, NBS Circ. 573, U.S. Government Printing Office, Washington 25, D.C. (June 26, 1956).

Johler, J. R., and L. C. Walters, Propagation of a ground wave pulse around a finitely conducting spherical earth from a damped sinusoidal source current, IRE Trans. on Antennas and Propagation **AP–7,** No. 1, 1–10 (Jan. 1959).

Johler, J. R., and L. C. Walters, On the theory of reflection of low- and very low-radio-frequency waves from the ionosphere, J. Research NBS **64D** (Radio Prop.), No. 3, 269–285 (May–June 1960).

Johler, J. R., L. C. Walters, and J. D. Harper, Jr., Low- and very low-radiofrequency model ionosphere reflection coefficients, NBS Tech. Note 69 (PB161570), U.S. Dept. of Commerce, Office of Technical Services, Washington 25, D.C. (July 1, 1960).

Johler, J. R., L. C. Walters, and C. M. Lilley, Low- and very low-radiofrequency tables of ground wave parameters for the spherical earth theory: The roots of Riccati's differential equation, NBS Tech. Note 7 (PB 151366), U.S. Dept. of Commerce, Office of Technical Services, Washington 25, D.C. (Feb. 1, 1959).

Johler, J. R., L. C. Walters, and C. M. Lilley, Amplitude and phase of the low- and very low-radiofrequency ground wave, NBS Tech. Note 60 (PB161561), U.S. Dept. of Commerce, Office of Technical Services, Washington 25, D.C. (June 1, 1960).

Lorentz, H. A., The theory of electrons and its applications to the phenomena of light and radiant heat (G. E. Stechert and Co., New York, N.Y., 1906, 1923).

Magnetic Chart 1706 N, The variation of the compass for the year 1955 North Polar area, U.S. Navy Hydrographic Office, Washington, D.C. (1946); 3rd edition (1954).

Magnetic Chart 1700 N, The magnetic inclination or dip for the year 1955 North Polar area, U.S. Navy Hydrographic Office, Washington, D.C. (1946); 3rd edition (1954).
Magnetic Chart 1703 N, The total intensity of the Earth's magnetic field for the year 1955 North Polar area, U.S. Navy Hydrographic Office, Washington, D.C., (1947); 2nd edition (1954).
Millington, G., Ground-wave propagation across a land/sea boundary, Nature **164,** 114–115 (July 1949); Nature **163,** p. 128 (June 1949).
Millington, G., Ground-wave propagation over an inhomogeneous smooth earth, Proc. IRE **96,** pt III, 53–63 (1949).
Nicolet, M., Aeronomic conditions in the mesosphere and lower ionosphere, Science Report No. 102, Pennsylvania State University, University Park, Pennsylvania (April 1958).
Rabinowitz, P., and G. Weiss, Tables of abscissas and weights for numerical evaluation of integrals of the form

$$\int_0^\infty e^{-x} x^n f(x)\,dx,$$

Mathematical Tables and Other Aids to Computation, Vol. 13, No. 68, p. 285 (Oct. 1959).
Ratcliffe, J. A., Ionizations and drift in the ionosphere, J. Geophys. Research **64,** No. 12, 2102–2111 (Dec. 1959).
Ross, J. M., Propagation field test, Appendix D (uncl.), Navigation, guidance and control system for drone aircraft, 6th Quarterly Progress Report to U.S. Army Signal Research and Development Laboratory, Ft. Monmouth, N.J. (Sept.–Nov. 1959), Contract No. DA 36–039 SC–78020, Motorola, Inc., Scottsdale, Arizona.
Seddon, J. C., and J. E. Jackson, Rocket arctic ionospheric measurements, IGY Rocket Report Series, No. 1, pp. 140–148 (July 1958).
Wait, J. R., Diffractive corrections to the geometrical optics of low frequency propagation, Electromagnetic wave propagation, pp. 87–101 (Academic Press, New York, N.Y., 1960a).
Wait, J. R., private communication, eq. (37), (1960b).
Wait, J. R., A diffraction theory for LF sky wave propagation, J. Geophys. Research **66,** No. 6, 1713–1730 (June 1961).
Wait, J. R., and A. M. Conda, Pattern of an antenna on a curved lossy surface, IRE Trans. on Antennas and Propagation **AP–6,** No. 4, 348–359 (October 1958).
Watt, A. D., E. L. Maxwell, and E. H. Whelan, Low-frequency propagation paths in artic areas, J. Research NBS **63D** (Radio Prop.), No. 1, 99–112 (July–Aug. 1959).
Waynick, A. H., The present state of knowledge concerning the lower ionosphere, Proc. IRE **45,** No. 6, 741–749 (June 1957).

(Paper 65D5-156)